

Coupling of forward osmosis with desalination technologies: System-scale analysis at the water-energy nexus

*Original*

Coupling of forward osmosis with desalination technologies: System-scale analysis at the water-energy nexus / Giagnorio, Mattia; Morciano, Matteo; Zhang, Wenjing; Hélix-Nielsen, Claus; Fasano, Matteo; Tiraferri, Alberto. - In: DESALINATION. - ISSN 0011-9164. - 543:(2022), p. 116083. [10.1016/j.desal.2022.116083]

*Availability:*

This version is available at: 11583/2971328 since: 2022-09-15T17:01:30Z

*Publisher:*

Elsevier

*Published*

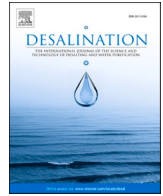
DOI:10.1016/j.desal.2022.116083

*Terms of use:*

This article is made available under terms and conditions as specified in the corresponding bibliographic description in the repository

*Publisher copyright*

(Article begins on next page)



# Coupling of forward osmosis with desalination technologies: System-scale analysis at the water-energy nexus

Mattia Giagnorio<sup>a,1,\*</sup>, Matteo Morciano<sup>b,c,1,\*</sup>, Wenjing Zhang<sup>a</sup>, Claus Hélix-Nielsen<sup>a</sup>,  
Matteo Fasano<sup>b,c</sup>, Alberto Tiraferri<sup>c,d</sup>

<sup>a</sup> Technical University of Denmark, Department of Environmental and Resource Engineering, Miljøvej 113, Kgs. Lyngby 2800, Denmark

<sup>b</sup> Politecnico di Torino, Department of Energy, C.so Duca degli Abruzzi 24, Torino 10129, Italy

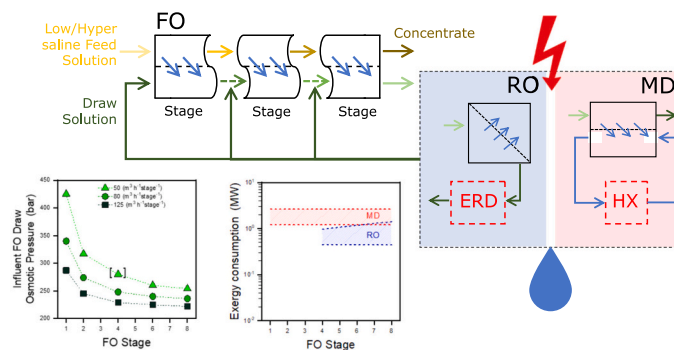
<sup>c</sup> Politecnico di Torino, Clean Water Center, C.so Duca degli Abruzzi 24, Torino 10129, Italy

<sup>d</sup> Politecnico di Torino, Department of Environment, Land and Infrastructure Engineering, C.so Duca degli Abruzzi 24, Torino 10129, Italy

## HIGHLIGHTS

- FO-RO and FO-MD desalination systems are investigated at the water energy nexus.
- Multi-stage operation is a valuable solution for co-current FO large-scale systems.
- FO-RO is ~100-fold more energy-efficient than FO-MD in low saline water treatment.
- FO-MD system is more flexible than FO-RO, able to work with extended salinity levels.
- FO-RO and FO-MD exergy consumption are comparable when treating hyper saline water.

## GRAPHICAL ABSTRACT



## ARTICLE INFO

### Keywords:

Forward osmosis  
Reverse osmosis  
Membrane distillation  
Multi-stage approach  
Energy consumption

## ABSTRACT

Couplings of forward osmosis (FO) with reverse osmosis (RO) or membrane distillation (MD) are investigated at the water-energy nexus. The treatment of low and hypersaline feed solutions was assessed, followed by discussion of the most effective hybrid scheme for different conditions. Two FO configurations are presented, suggesting the potential applicability of a versatile multi-stage approach for treating low-saline wastewater sources under co-current membrane module design. Subsequently, energy and exergy consumption of the post-treatment RO / MD were evaluated. Finally, the coupling of FO and RO or MD units is investigated, highlighting the dependence of the two hybrid systems upon the operating parameters in FO. While FO-RO coupling is the most efficient solution in terms of power and exergy consumption, it is narrowed by the choice of the salinity gradient in the draw solution. A 2 order of magnitude higher power consumption is required by the MD to drive back the draw solution in FO while treating low saline wastewater. When dealing with hypersaline solutions instead, the FO-MD becomes more competitive, mostly from the exergy standpoint, highlighting the ability to use low-grade heat. Overall, FO-MD is more versatile, showing a broader application range while potentially approaching zero liquid discharge.

\* Corresponding authors.

E-mail addresses: [matgi@env.dtu.dk](mailto:matgi@env.dtu.dk) (M. Giagnorio), [matteo.morciano@polito.it](mailto:matteo.morciano@polito.it) (M. Morciano).

<sup>1</sup> These two authors contributed equally to this work.

## 1. Introduction

Forward osmosis is widely recognized as a valuable alternative desalination process, in which the natural process of osmosis is engineered to extract high-quality water from contaminated streams by means of a draw solution (DS) able to establish an osmotic gradient at the membrane interface [1]. In detail, forward osmosis represents an especially promising technology for the treatment of complex water streams [2–5]. Contrary to pressure-driven membrane systems, the absence of an external applied hydraulic pressure gives the possibility to process, in FO, water sources with organic and suspended solid contents [4,6] and to reduce the cost of installation by using fully polymeric materials. Moreover, the potential deployment of a variety of draw solutes makes the FO a versatile technology, able to treat feed solutions with either low or hyper salinity levels [7–10].

Forward osmosis may be deployed as stand-alone membrane system, virtually with no or little requirement of an external energy input to drive the permeation process. In this case, named osmotic dilution (OD) or osmotic concentration, the draw solution is used to extract water from the feed stream without requiring a further downstream recovery step. This configuration has been mainly reported for medical applications or for direct fertigation, whereby engineered draw solutes are diluted via OD prior to their beneficial use [11,12]. An attractive OD configuration consists of the utilization of natural draw solutions to drive the permeation process. Thanks to its intrinsic characteristics, seawater is considered a valuable draw solution to extract water from feed solutions with low total dissolved solids concentrations [13].

Comprehensive studies have been performed to investigate, e.g., potential alternative draw solutions in FO or the changes in membrane module configuration [14,15]. Recently, studies have assessed FO feasibility in situ (e.g., treating real water sources or investigating possible pilot configurations) to close the gap between lab and real scale applications [16–18]. However, this is still a largely uncharted territory and research is necessary to assess the implementation of forward osmosis systems in large scale applications, as well as the integration of the FO step with post-recovery systems. In this regard, it is indeed essential to emphasize that, aiming at zero liquid discharge and at a general minimization of waste within the water treatment sector, forward osmosis requires a downstream desalination technology able to process the diluted draw solution, separating the draw solute from the water extracted in the FO step, thus continuously restoring the draw solute concentration [19,20]. In this configuration, energy is required to drive the subsequent desalination system, usually represented by either a pressure-driven or a thermally-driven process.

The choice of the coupling technology is governed by the characteristics of the draw solute as well as by the salinity gradient driving the FO permeation step. Studies proposed and assessed potential FO implementations, with nanofiltration (NF), reverse osmosis (RO) and membrane distillation (MD) being the best candidates for draw solution recovery. Currently, pressure-driven membrane processes (NF/RO) represent the most energy efficient options [21]. However, the concentration of draw solution that can be recovered with NF/RO, hence, the salinity of the primary feed stream, is narrow, in turn limiting the versatility of the coupling technology. In detail, the current maximum operating pressure for commercial RO membrane modules is around 80 bar [22], with a few studies reporting the possibility to reach up to 100 bar [23]. Treating hypersaline solutions is challenging considering the current limitations related to membrane materials, module packing, topology, and fouling/scaling phenomena. Therefore, the mechanical integrity and a proper permeability may not be guaranteed. For this reason, FO-NF/RO was reported so far in the literature as a promising solution for the treatment of low-salinity wastewater and groundwater sources [16,24].

An emerging alternative, which has been recently gaining ground, is represented by FO coupled with MD. The latter is particularly promising due to its ability to perform low-temperature separation with low-grade

energy, such as industrial and non-industrial waste heat, as well as renewable energy sources [25–29]. Furthermore, MD is a suitable option for draw solution recovery as it allows the management of high salinity waters, being less sensitive to the variation of the solute concentration [19,22,30–32] while showing low fouling propensity [22]. In fact, contrary to pressure-driven membrane systems, the driving force in MD process is the partial pressure difference of the vapor generated across the membrane, i.e., between the feed solution to be treated (the diluted DS in FO-MD configurations) and the distillate. Such partial pressure difference shows a relatively low dependence on salinity (see Raoult's law [32]). Previous studies indicated that the upper operating limit of salinity of the feed solution is 200,000 ppm [22,23]. As a result, FO-MD has been mostly investigated when hypersaline draw solutions were needed to drive the FO permeation step [33–37]. On the other hand, there is a lack of understanding of FO-MD coupling, especially when considering the major limitation of MD, namely the low water recovery rate achievable in single stage operation mode [22].

Regarding the MD, most of the scientific activity conducted throughout the years was focused on optimizing the heat and mass transfer phenomena across the hydrophobic membrane. Solving this system of non-linear heat and mass transfer equations involves extensive computational efforts. However, developing a simplified, but accurate, mathematical model able to faithfully estimate the performance of such technology is highly desirable in order to effortlessly explore its potential coupling with forward osmosis, thus moving from component to plant-scale modeling. On this point, it is worth noting that a pioneering framework for evaluating the inherent potential thermodynamic performance of the MD process has been recently proposed and established by Christie and co-workers [38].

The study proposed here investigates the possible implementation of FO-RO/MD hybrid systems by performing a system-scale analysis at the water-energy nexus. Firstly, FO configurations are assessed, evaluating the influence of different operating parameters and multi-stage arrangements on water extraction from potential contaminated streams. In detail, the FO analysis is performed by discretizing the membrane systems while calculating the water filtered during the process. Then, with the aim of coupling the RO/MD technologies with the FO plant, the specific energy and exergy consumption related to RO/MD post-processes are calculated. For the sake of comprehensiveness, couplings between FO and both low- and unconventional high-pressures (namely, applied pressure lower than 100 bar and from 100 to 300 bar, respectively) RO (LPRO & HPRO), able to regenerate also hypersaline draw solutions, are included for comparison. Moreover, with regard to the MD technology, both a basic and an advanced configuration are considered. The advanced configuration incorporates a heat exchanger recovering the latent heat from the permeate stream to preheat the feed stream. Then, in order to evaluate the specific energy consumption of the MD process, the inspiring and simplified approach proposed by Christie and co-workers [38] is here considered and tailored to properly fit the hybrid configurations explored. In addition, the equations for evaluating the non-uniform trans-membrane temperature difference across the module are here included and discussed. Finally, the power required to restore the concentration of the draw solute, as well as the exergy consumption, are calculated for several hybrid case studies involving couplings between different multi-stage configurations of FO, RO and MD, different draw solutions flow rate per stage and osmotic pressure.

## 2. Methods

### 2.1. Forward osmosis

Simulations were performed considering three different case scenarios, namely, (i) forward osmosis for civil wastewater treatment - FOCW, considering an overall water recovery of 85 %, (ii) osmotic dilution for civil wastewater treatment - ODCW, considering an overall water recovery of 85 % and (iii), forward osmosis for the treatment of

hypersaline Water sources - FOHW, considering an overall water recovery of 60 %. Based on the results achieved in previous experiments [39], in FOCW,  $MgCl_2$  was considered as the most suitable draw solute, differently from the ODCW scenario, in which seawater was simulated as DS. In the FOHW case study, sodium propionate (NaPRO) was deployed as draw solute, given the promising results discussed by previous studies [36]. While the operating conditions may vary in the two FO scenarios depending on the concentrations of  $MgCl_2$  or NaPRO considered for the draw solution, seawater was modeled considering a representative concentration of  $35 \text{ g L}^{-1}$  of NaCl in OD. In the latter case, a potentially infinite DS volume could be virtually up taken from the sea, while total DS volumes need to be optimized when working with engineered solutions in the two forward osmosis cases. This is necessary to keep reasonable operating costs while lowering the associated environmental impacts. Civil wastewater was simulated according to our previous literature works [39,40], without considering any foulant concentrations and by simplifying the mixture of ionic species with an equivalent NaCl concentration providing an osmotic pressure of 0.5 bar. The brine produced by a reverse osmosis seawater desalination system with an average water recovery of 50 % was considered as hypersaline water source.

System-scale analysis of forward osmosis and osmotic dilution was performed by simulating the potential configurations reported in Fig. 1a and S2. The FO and OD configurations consisted of different stages, each supplied with specific volume and mass flow rates of feed and draw solution. While the feed is treated sequentially along the stages, i.e., the concentrate of one stage is the feed of the following one, the influent draw solution of each stage was designed following two potential system configurations. The first one (Conf1 along the manuscript), depicted in Fig. S2, was only used to simulate the FOCW scenario. Here, the total flow rate of the  $MgCl_2$  draw solution is divided equally among the various FO stages, in which the permeation is driven by the re-concentration factor obtained by mixing the diluted draw solution exiting the previous stage and the new influent DS flow. The second configuration (Conf2 along the manuscript), reported in Fig. 1, is designed in a way that each of the stages receive a fresh draw solution source. This configuration was used to simulate all three scenarios described above, thus varying the source of draw solution accordingly.

A downstream desalination technology is necessary for the draw solution regeneration in the FO cases, while no post-treatment is contemplated in osmotic dilution mode. Potentially, the OD system can be combined with a reverse osmosis unit to extract water from the diluted seawater draw solution, thus increasing the recovery rate of the RO desalination step. This case scenario was not investigated in this study, since previous research already proved the potential benefits of this coupled strategy [20,41]. However, an in-depth investigation of innovative osmotic dilution configurations is of interest. Binger et al. [42] reported an in-depth investigation of a multi-stage approach in FO, focusing on the influence of the membrane module parameters on the water permeation when a wastewater source is used to dilute seawater prior to operate the subsequent reverse osmosis desalination step. It is of interest to investigate additional similar configurations with a broader perspective, falling outside specific membrane module analysis and evaluating FO scenarios at the system-level and the related energy needs associated with the deployment of different post-recovery solutions.

The system-scale analysis was performed by discretizing the theoretical length of each membrane stage while calculating the water flux  $J_w$ . Thus, the dilution factor of the draw solution, the reverse salt flux through the membrane  $J_s$ , and the concentration factor of the feed solution were considered. The values of the active layer water permeance (A), the support layer structural parameter (S), as well as the salt permeability coefficient (B) for each draw solute and its related diffusion coefficient (D) were taken from previous measurements reported in the literature [34,39]. For each draw solute, the correlation between the variation of the osmotic pressure in solution and the solute concentration were extrapolated using OLISystem Analyser. The discretization of

each membrane stages was performed in 2D geometry, accounting for a mass transfer coefficient equal to what reported in our previous studies [34,39]. To simplify the analysis, simulations were first performed in co-current configuration (i.e., feed and draw solutions entering and exiting from the same sides) and subsequently in counter-current configuration, in the latter case fixing the recovery rate of the system based on the results obtained in co-current mode. Co- and counter-current representations are reported in the Supporting Information (Fig. S1).  $J_w$  and  $J_s$  were calculated through the following equations [43]:

$$J_w = A \left\{ \frac{\pi_D e^{\left(\frac{-J_w \Delta S}{D}\right)} - \pi_F e^{\left(\frac{J_w \Delta S}{D}\right)}}{1 + \frac{B}{J_w} \left[ e^{\left(\frac{J_w \Delta S}{D}\right)} - e^{\left(\frac{-J_w \Delta S}{D}\right)} \right]} \right\} \quad (1)$$

$$J_s = B \left\{ \frac{c_{DS} e^{\left(\frac{-J_w \Delta S}{D}\right)} - c_{FS} e^{\left(\frac{J_w \Delta S}{D}\right)}}{1 + \frac{B}{J_w} \left[ e^{\left(\frac{J_w \Delta S}{D}\right)} - e^{\left(\frac{-J_w \Delta S}{D}\right)} \right]} \right\} \quad (2)$$

where  $c_{DS}$  and  $c_{FS}$  are the draw and feed solutions concentration, respectively.

Note that the energy consumption in the FO step was considered negligible compared to the energy associated with the downstream desalination technologies. This assumption is mostly based on the observation that the direct energy consumption in FO is only associated with the head losses within the system, which are negligible compared to the energy required to achieve high pressures or related to the heat to be supplied to the following RO/MD systems.

## 2.2. Specific energy consumption of reverse osmosis

The methodology adopted for calculating the specific energy consumption (i.e., SEC) of RO, which is the pressure-volume work to produce a  $\text{m}^3$  of permeate, is discussed. Two typical case studies are considered for this purpose: the conventional single-stage configuration and the multi-stage configuration (where the brine solution exiting the first stage enters as feed solution into the second stage and so on), which offers benefits from an energy standpoint. In fact, while in the former configuration the applied pressure is constant throughout the vessels, resulting in a pressure difference at the vessel inlet significantly higher than theoretically required, the multi-stage configuration allows working with a gradually increasing pressure that matches the increase in brine osmotic pressure [44]. In both configurations, the use of an energy recovery device is included in the calculations. The efficiency of this component, which is designed to recover as much mechanical energy as possible from the high-pressure and high-concentrated brine [45,46] (indicated as  $P_R$  in Fig. 1), significantly affects the total specific energy consumption [23,47–49].

The analytical equations used to calculate the intrinsic specific energy consumption of the RO process are outlined below. These equations are obtained assuming the efficiency of the pump  $\eta_{pump} = 0.8$ , the efficiency of the energy recovery device (i.e., ERD [50], which could be pressure exchangers or turbines [23])  $0.8 \leq \eta_{ERD} \leq 1$  and an excess of hydraulic pressure at the outlet of each stage  $\Delta p_{out}$  equal to 10 bar above the osmotic pressure of the brine exiting the stage. The applied hydraulic pressure ranges from 25 to 300 bar, based on the detailed considerations reported in Ref. [23]. In detail, the lower selected limit corresponds to the pressure suitable for processing wastewater with low concentration levels (i.e. less than  $35 \text{ g L}^{-1}$ ). The upper limit is needed to overcome the osmotic pressure of hypersaline brines, which can be treated by the so-called high-pressure RO systems with applied pressures higher than 100 bar [23]. In detail, an hydraulic pressure of 300 bar enables brine concentrations up to  $250,000 \text{ mg L}^{-1}$ , which is challenging considering the limitations related to the membrane materials and the fouling phenomena. Given the selected concentration range, The van't Hoff equation provides reasonable accuracy between solute concentration and

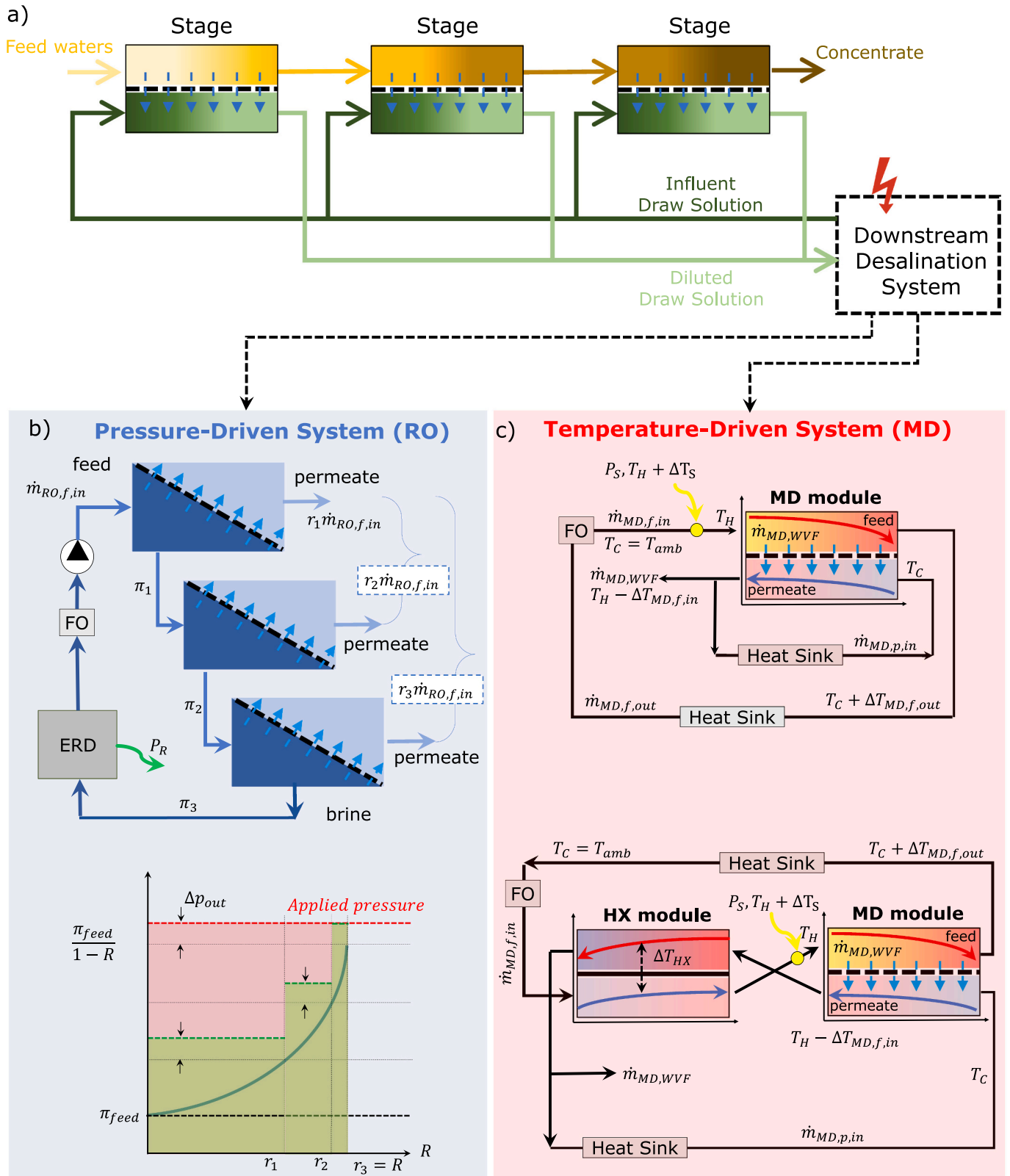


**Fig. 1.** Schematic representation of the configurations designed for potential large-scale forward osmosis (FO) applications. a) Coupling between multi-stage FO plant and a downstream desalination system able to restore the concentration of the influent draw solution. The downstream desalination systems considered in this work are based on b) reverse osmosis (RO) and c) membrane distillation (MD) processes. With respect to the RO process, two implementation arrangements were considered, namely, the single and multi-stage configurations. In the figure, a 3-stage configuration is reported for the sake of conciseness. Furthermore, a device for recovering the mechanical energy (ERD) stored in the brine is considered. With respect to the MD process, the two arrangements differ from the presence of a heat exchanger (HX) able to preheat the feed stream entering the MD module by recovering the heat stored in the permeate stream. In the figure, a single stage recovery is reported, although multiple identical stages may be coupled in series to achieve the desired recovery.

osmotic pressure for values below 200 bar. For the upper range, OLI-System Analyser was used to check the validity of the van't Hoff equation and to replace values with more accurate ones if needed. Furthermore, salt rejection is considered as ideal (higher than 99 % in practical real cases). As a result of these considerations, the brine osmotic pressure  $\pi_{brine}$  can be written as a function of the feed osmotic pressure  $\pi_{feed}$  and a fixed target recovery  $R$  as:

$$\pi_{brine} = \frac{\pi_{feed}}{1-R} \quad (3)$$

Then, the following is the equation that was used to evaluate the specific energy consumption  $SEC$  of a RO process in the case of a single-stage [23]:

$$SEC_{N=1} = \frac{\left(\frac{\pi_{feed}}{1-R} + \Delta p_{out}\right)(1 - (1-R)\eta_{ERD})}{\eta_{pump}R} \quad (4)$$

When dealing with a multi-stage configuration, the osmotic pressures and the cumulative recovery rates at the end of each  $i$ -th RO stage (indicated as  $\pi_i$  and  $r_i$ , respectively) are equal to [47]:

$$\pi_i = \left(\frac{\pi_{feed}}{1-R}\right) \left(1 - \left(\frac{N-i}{N}\right)R\right) \quad (5)$$

$$r_i = 1 - \frac{\pi_{feed}}{\pi_i} \quad (6)$$

where  $N$  represents the number of stages. Thus, the various stages of the RO process deal with progressively higher osmotic feed pressure (i.e.,  $\pi_i$ ) and progressively lower mass flow rates compared to the upstream stages. Following, the equation for the  $SEC$  of a RO process, in case of a 3-stage, is reported:

$$SEC_{N=3} = \frac{\pi_1 + \Delta p_{out} + \sum_{i=1}^{N-1} (1-r_i)(\pi_{i+1} - \pi_i)}{\eta_{pump}R} - \frac{(1-R)\eta_{ERD}(\pi_3 + \Delta p_{out})}{\eta_{pump}R} \quad (7)$$

### 2.3. Specific energy consumption of membrane distillation

Here, the methodology adopted for calculating the specific energy consumption of MD to produce a  $m^3$  of permeate is discussed. The reported methodology is inspired by the pioneering work recently authored by Christie and co-workers [38], where a streamlined framework for evaluating the inherent potential thermodynamic performance of the MD process was established [38]. Without losing generality, a counter-current (see Fig. 1) direct contact membrane distillation (DCMD) process was considered. Moreover, two configurations were explored: a configuration in which the outflow from the permeate channel of the MD module is conveyed directly back into the FO unit, after thermalizing it with the environment by means of a heat sink (see Fig. 1a); a configuration involving a heat exchanger (HX) to preheat the feed stream entering the MD module by recovering the residual heat in the permeate stream (see Fig. 1b).

Here we focus on quantifying the inherent potential performance of an MD desalination system used as downstream separation step of FO. In particular, we explore the effect of thermal efficiency  $\eta_{mem}$ , inlet temperature of the streams in the feed and permeate channel (i.e.,  $T_H$  and  $T_C$ , respectively; whose difference is indicated as  $\Delta T$ ), trans-membrane temperature difference at the output or input section of the feed channel (i.e.,  $\Delta T_{MD, f, out}$  or  $\Delta T_{MD, f, in}$ , respectively), and temperature difference between the hot and cold streams along the heat exchanger (i.e.,  $\Delta T_{HX}$ ) on the MD performance.

To evaluate the intrinsic performance of the proposed MD process, the source of thermal energy  $P_S$  required to heat the solution entering the MD module (i.e., the FO draw solution) up to  $T_H$  is introduced. If the

heat exchanger is not involved in the design,  $P_S$  is:

$$P_S = c_f \dot{m}_{MD, f, in} (T_H - T_C) \quad (8)$$

where  $c_f$  is the specific heat of the feed solution and  $\dot{m}_{MD, f, in}$  is the total mass flow rate entering the feed channel of the MD module. The thermal efficiency  $\eta_{mem}$  is given by the ratio between the heat transferred through water vapor flux  $\dot{m}_{MD, WVF}$  across the membrane and the total heat carried by the feed mass flow rate  $\dot{m}_{MD, f, in}$  (undergoing a temperature change from  $T_H$  to  $T_C - \Delta T_{MD, f, out}$ ), namely:

$$\eta_{mem} = \frac{\dot{m}_{MD, WVF} h_{vap}}{c_f \dot{m}_{MD, f, in} (T_H - T_C - \Delta T_{MD, f, out})} \quad (9)$$

where  $h_{vap}$  is the enthalpy of vaporization. Finally, the specific thermal energy consumption is:

$$SEC_I = \frac{P_S}{\dot{m}_{MD, WVF}} \quad (10)$$

Combining Eqs. (8), (9) and (10), we get:

$$SEC_I = \frac{\Delta T h_{vap}}{(\Delta T - \Delta T_{MD, f, out}) \eta_{mem}} \quad (11)$$

Considering a design in which the HX is included (see Fig. 1b), previous equations can be re-written as:

$$P_S = c_f \dot{m}_{MD, f, in} (T_H - (T_H - \Delta T_{MD, f, in} - \Delta T_{HX})) \quad (12)$$

$$SEC_{I, HX} = \frac{(\Delta T_{MD, f, in} + \Delta T_{HX}) h_{vap}}{(\Delta T - \Delta T_{MD, f, out}) \eta_{mem}} \quad (13)$$

It is worth pointing out that the theoretical framework developed here also considers that the trans-membrane temperature at the inlet section of the MD module (i.e.,  $\Delta T_{MD, f, in}$ ) differs from that at the outlet section (i.e.,  $\Delta T_{MD, f, out}$ ), being related by the first law of thermodynamics on the MD module:

$$\begin{aligned} &\dot{m}_{MD, f, in} c_f (T_H - T_{ref}) + \\ &-\dot{m}_{MD, f, out} c_f (T_C + \Delta T_{MD, f, out} - T_{ref}) = \\ &= \dot{m}_{MD, p, out} c_p (T_H - \Delta T_{MD, f, in} - T_{ref}) + \\ &-\dot{m}_{MD, p, in} c_p (T_C - T_{ref}) \end{aligned} \quad (14)$$

where  $c_p$  is the specific heat of the permeate solution. Note that Eq. 14 is valid for both configurations in Fig. 1c. Then, considering an equal inlet heat capacity of the streams in the feed and permeate channels of the MD module [38], we get:

$$\begin{aligned} &\Delta T_{MD, f, in} \left(1 + R \frac{c_p}{c_f}\right) - \Delta T_{MD, f, out} (1 - R) = \\ &= R \left(\frac{c_p}{c_f} T_H - T_C\right) \end{aligned} \quad (15)$$

For the sake of conciseness, the reference temperature term (i.e.,  $R T_{ref} (1 - c_p/c_f)$ ) does not appear in Eq. 15, being negligible with respect to the operating temperatures.

We then proceed to analyze the specific performance of the MD technology from an exergetic point of view as well [51,52]. The specific thermal exergy consumption ( $SEC_{II}$ ), defined as the amount of exergy supplied to produce a volume of distillate, can be similarly derived by including the Carnot factor [27,28,51]:

$$\eta_{Carnot} = 1 - \frac{T_{amb}}{T_H + \Delta T_S} \quad (16)$$

where,  $\Delta T_S$  is the difference between the temperature of the low-grade thermal source and the inlet temperature of the streams in the feed channel (i.e.,  $T_H$ ). Thus, the exergy associated with a given quantity of heat flux and employed to produce a unit volume of distillate is  $SEC_{II} = \eta_{Carnot} SEC_I$  [28,51]. The thermal source may come from flat plate solar

collectors or waste heat recovery. Note that the temperature of the dead state corresponds to the ambient temperature (i.e.,  $T_{amb}$ ).

### 3. Results

#### 3.1. Preliminary FO simulations

Forward osmosis simulations were performed to investigate the feasibility of the system configurations in co- and counter-current mode. The same case scenario was considered to carry out the modeling analysis, i.e., FOCW. All the results are presented in the Supporting Information, Fig. S3, showing the trend of the water flux along the FO stages as function of the recovery rate.

Results suggest that Conf1 does not represent an advantageous configuration for FO. Lower water fluxes would be achieved within the membrane stages compared to the one stage permeation (results shown for co-current operation in Fig. S3a). The unsuitability of such configuration is in line with our previous modeling analysis [39,40], being mainly ascribed to the lower DS to FS volume ratio reached in each stage of the system, which increases the dilution factor of the draw solution along the membrane length. Even a re-concentration step carried out prior to each permeation stage by mixing the diluted DS with fresh DS volume is not sufficient to increase the water flux. As opposed to an RO process, for which dividing the membrane in multiple stages leads to better thermodynamic performance, in FO the loss of driving force due to dilution in each stage plays a much more important role. Unless the total flow rate of draw solution (i.e. the mass of draw solute) is increased significantly in the system, using a multi-stage arrangement is not particularly advantageous.

The modeling analysis also suggests that no significant optimization would be achieved when working with the two configurations in counter-current mode. An overall decrease in productivity was achieved in Conf1 (results not shown), similar to what observed by simulating the permeation in co-current. Interestingly, a significant variation of the water flux trend would be achieved if counter-current is adopted in Conf2 (Fig. S3b). Specifically, a multiple stage approach would significantly reduce the water flux stability along the recovery. This result is mainly ascribed to the nature of the counter-current mode, where the more concentrated draw solution is always associated to a more concentrated feed solution along the membrane, therefore providing the correct amount of driving force capable to determine a more balanced and stable permeation with a single stage membrane system configuration. It could be said that a single-stage counter-current FO process is analogous to a multi-stage RO process with gradually increased applied hydraulic pressure, at least in terms of achieving flux balance and optimizing the use of driving force.

Interesting observations can be made by performing a system-scale analysis to calculate the theoretical variation of cross-flow channel height needed in the FO membrane module to maintain a uniform cross-flow velocity (Fig. S4). Overall, while in counter-current a more stable flux is produced along the membrane module, a theoretical large variation of the cross-flow channel thickness would be necessary to keep a uniform cross-flow velocity (Fig. S4d). This is due to the large increase in the flow rates along the membrane module in the same direction for both the feed and the draw solution, i.e., large flow rates at one end of the module and small flow rates at the other end (Fig. S4b). This effect would require complex modules geometry to minimize the concurrent change in both cross-flow velocities. An increase in the cross-flow velocity would strongly affect the water and solute transfer through the membrane while inducing turbulent flow conditions at the membrane surface. This may not necessarily have a negative impact on the membrane performance, but would ideally require adjustments in module design or structure, or would otherwise impose stricter operating limits to the deployment of the FO modules, e.g., minimum and maximum cross-flow rates. Designing modules or processes to work within specific range of recovery rates, cross-flow rates and velocities, as well as

influent DS:FS flow rates is essential to keep a modular structure and guarantee robustness of performance and long component service life in large scale applications.

The need for highly-efficient geometry is less pronounced in FO modules working in co-current mode, where the increase of DS flow rate due to dilution is counter-posed by the corresponding volume reduction of the feed flow, resulting in a theoretical uniform section of the membrane module along with the area (Fig. S4c). To make an example, in co-current, the traditional cylindrical shape of spiral wound or hollow fiber modules may be maintained, potentially adopting less stringent operative limits than those needed for a counter-current module. However, this may be obtained at the expense of a less uniform water flux in single stage configuration.

#### 3.2. Staged operation in FO

The results reported so far suggest: (i) the inefficiency of Conf1 when working in forward osmosis, and (ii) the unfeasible re-design of counter-current systems in multiple stage operation. However, co-current FO membrane modules may be favorably assembled by designing systems according to Conf2 (Fig. 1a). This is shown by the results and discussion reported in the following section.

First, simulations were performed to investigate the FOCW and FOHW scenarios. The modeling analysis was carried out by fixing the recovery rate of the entire system to 85 % and 60 %, respectively. Results are presented in Fig. 2. The water flux trend achievable along the stages is reported in Fig. 2a and Fig. 2c for the FOCW and FOHW case study, respectively.

In FOCW, a counter-current single stage configuration is able to produce a more stable water flux along the plant and better exploit the driving force, thus representing the most valid operational approach when a traditional single stage configuration is adopted. This is ascribed to a more uniform trend of the concentration gradients between the feed and the draw solution along the membrane system. This is an expected results and in accordance with previous analysis [39]. Interestingly, results suggest that co-current FO may be adjusted by designing a multi stage system accordingly to Conf2, thus representing a possible alternative to the traditional counter-current approach. Compared to the single stage permeation, this multi-stage operation would bring benefits to the membrane systems by reducing the maintenance cost related to the potential difference in fouling that would probably be associated with a large variation of the water flux along the membrane (see Fig. 2a). Moreover, a Conf2-based system may represent a feasible option for the treatment of more complex wastewater, containing large concentration of foulants combined with high silt density index (such as liquid fraction of digestate [6]). While FO can deal with the presence of suspended solids in solution, the increase in concentration of contaminants in the feed side may induce organic/inorganic precipitation onto the membrane, leading to irreversible fouling. A multi-stage approach can simplify the maintenance by operating directly within the fouled stage, while keeping unaltered the permeation conditions in the rest of the plant.

In contrast, when treating hypersaline sources, neither a co-current nor a counter-current approach would be able to obtain a stable and uniform water flux along the recovery rate of the permeation (and hence, along the membrane area), as shown in Fig. 2c. This is mainly due to the intrinsic higher salinity of the feed water and its concentration along the membrane modules. These results draw attention to unexpected issues that may arise during real-scale FO operations, which should be carefully designed in FOHW scenarios, keeping in mind the potential detrimental effect of a large water flux variation in membrane module performance and fouling.

It is worth noting that the FOCW and FOHW simulations were performed keeping the same feed solution to draw solution flow rate ratio, i.e., FS:DS = 1:2. However, a large variation in osmotic pressure difference was needed to drive the two FO scenarios. An influent DS osmotic

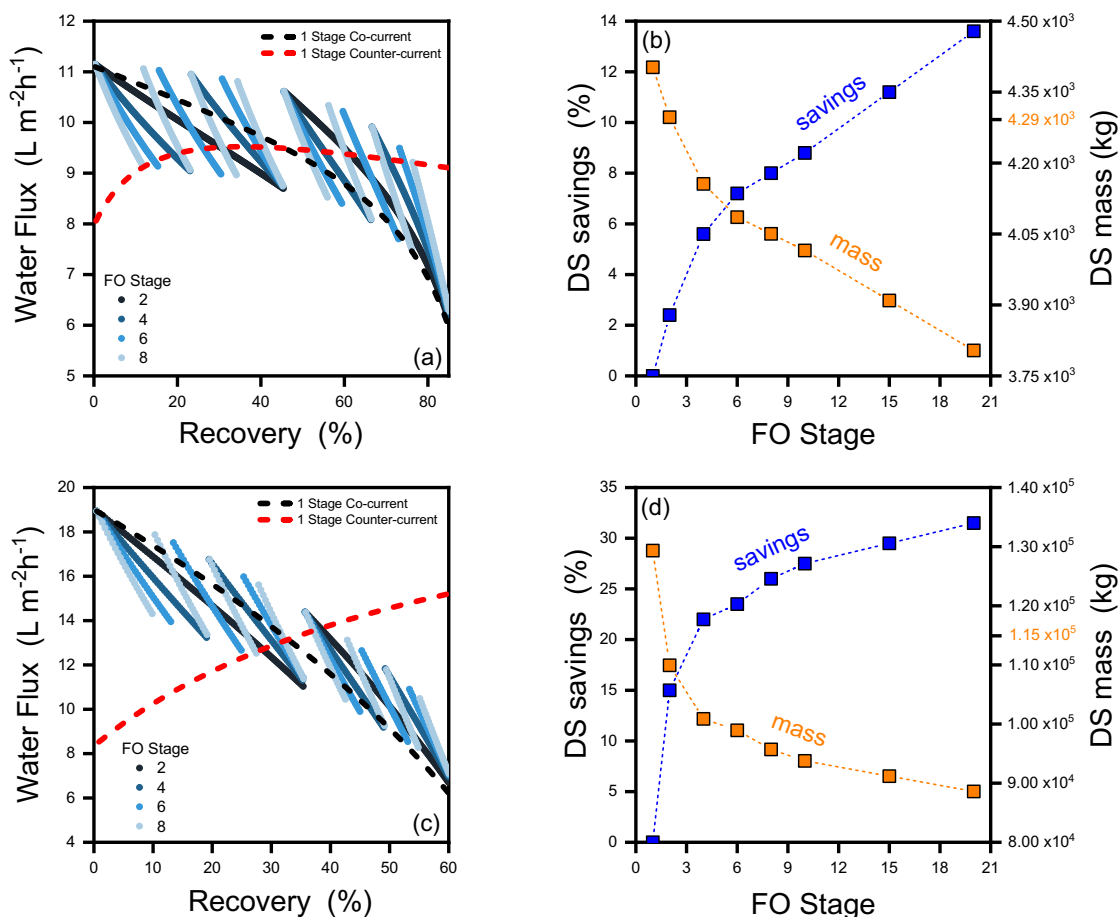


**Fig. 2.** Results of forward osmosis simulations performed to model the FOCW/FOHW scenarios. The FO system was designed based on Conf2, considering an (i) influent total  $\text{MgCl}_2/\text{NaPRO}$  DS volume of  $200 \text{ m}^3 \text{ h}^{-1}$ , (ii) an influent draw osmotic pressure of 16/280 bar and, (iii) local water fluxes always higher than  $5 \text{ L m}^{-2} \text{ h}^{-1}$  along the membrane area. The water flux trends a) and c) are reported as a function of the recovery rate while varying the number of stages. Dashed lines represent the co-current and counter-current simulations performed with single stage designs. Panels b) and c) report the variation of (i) the  $\text{MgCl}_2/\text{NaPRO}$  DS flow rate in percentage and (ii)  $\text{MgCl}_2/\text{NaPRO}$  DS mass as function of the number of FO stages included in the system design. Orange values in the right y axis indicate the draw solution mass needed to drive the two FO scenarios in single-stage counter-current mode.

pressure almost 14 times higher was required to reach a much lower (60 %) recovery rate in the FOHW scenario compared to the driving force needed to achieve 85 % recovery in FOCW, while keeping the local water fluxes always higher than  $5 \text{ L m}^{-2} \text{ h}^{-1}$  along the membrane area.

Interestingly, results suggest that in none of the cases discussed above, a no significant change in membrane area would be associated with the deployment of single or multi stage configuration to obtain the same overall recovery value. Therefore, a multi stage operation would not result in a significant increase (or decrease) of the installation costs in real scale plants. Instead, a multi stage approach in co-current operation would potentially lead to draw solution savings up to approximately 8 % and 23 % for 6 stages, as reported in Fig. 2b and d. With a multi stage configuration, a lower amount of draw solute may be deployed to achieve the same outcomes with a fixed plant size. This is evident in FOHW scenarios, whereby extreme concentrations of draw solutes are needed to drive the permeation of hypersaline water. When compared to the single stage co-current operation, this finding is partially relevant for the counter-current configuration too, as indicated by the orange values reported in the right y axis of Fig. 2b and d. It is worth noting that, in the presence of significant environmental burdens associated with the production and deployment of the chosen draw solute, even a small saving may lead to a more environmentally friendly membrane system [40].

All the simulations and results discussed above have an impact on the efficiency and energy requirements of the downstream step applied to

regenerate the draw solution. Indeed, different draw solution flow rates, as well as influent and effluent draw solute concentrations, are directly related to the operating conditions and size of the RO or MD processes that would need to treat these solutions. Therefore, multi-stage FO arrangements associated with lower or larger values of DS flow rates or concentrations with respect to single-stage FO would lead to potential savings for the overall coupled system. Note that the design of a multi-stage FO plant is not necessarily more complex or costly than that of a single-stage system. No pressure booster pumps or expensive materials are needed in FO, as opposed to, e.g., RO plants, and a multi-stage approach would simply translate in different piping entering and exiting the various membrane vessels, with extra costs only virtually related to low-pressure pumps and valves. While such calculations are not in the scope of this study, designing a rational multi-stage FO step may thus result in OPEX savings that would largely offset the possible increase in CAPEX costs, in addition to facilitating the implementation of more streamlined module structures or operating conditions, as discussed above.

### 3.3. Staged operation in OD

Modeling analysis was performed to simulate the ODCW scenario, in which no DS regeneration is needed. In this case study, the forward osmosis system was designed to ideally work in coastal areas, while using seawater as draw solution for the treatment of wastewater with

low total dissolved solids concentration. Considering the nature of the draw solution and, ideally, the possibility to uptake large amounts of seawater, the simulations were performed with a fixed volume of DS entering each stage (equal to  $200 \text{ m}^3 \text{ h}^{-1}$ , to be consistent with the simulations showed previously). It is worth noting that the multiple stage permeation systems in OD works with an amount of the total seawater DS proportional to the number of stages, differently from the forward osmosis scenarios, in which a fixed DS flow rate is equally divided among the stages involved.

The results of the simulations are reported in Fig. 3. The water flux in co-current (1 and multi stage) and counter-current (1 stage) is reported as function of the recovery rate (Fig. 3a). Overall, larger water fluxes can be achieved in co-current multi-stage operation, leading to potential savings in terms of plant size and, hence, installation costs (Fig. 3b). Clearly, the gap between the water flux trend between 1 and multiple stage configurations is more pronounced in ODCW compared to FOCW scenarios. This is due to the higher driving force combined with the larger DS flow rates involved when working with seawater as draw solute instead of an engineered DS, such as magnesium chloride. Results suggest that in 1 stage co-current mode, when treating civil wastewater with low salinity level, a large variation of the local water flux along the membrane module is observed (black dashed lines in Fig. 2a and b). This is ascribed to the large value of osmotic pressure difference between the feed and the draw side at the entrance of the module and the low value at the exit of the module (as feed water gets concentrated and draw solution diluted). In ODCW, a multi-stage configuration would hence represent a promising solution in co-current mode, achieving a more uniform water flux along the stages while reducing the environmental footprint of the system (Fig. 2b); the proportionally larger volumes of DS would not be an issue, given the large availability of seawater. As expected, similar uniformity in membrane performances can be obtained in 1-stage counter-current mode but at the expense of a lower average water flux, resulting in larger membrane area requirements to obtain the same recovery rate (Fig. 2b). It is worth mentioning that, in the presence of a reverse osmosis system used to recover the water extracted during the FO permeation step, larger volume of diluted draw solutions derived from a multi-stage operation approach would potentially affect the overall energy cost of the coupled technology. An analysis of the coupling of FO with desalination systems is reported below and the results may be adopted to derive the energy needs associated with the deployment of an osmotic dilution coupled with RO as well.

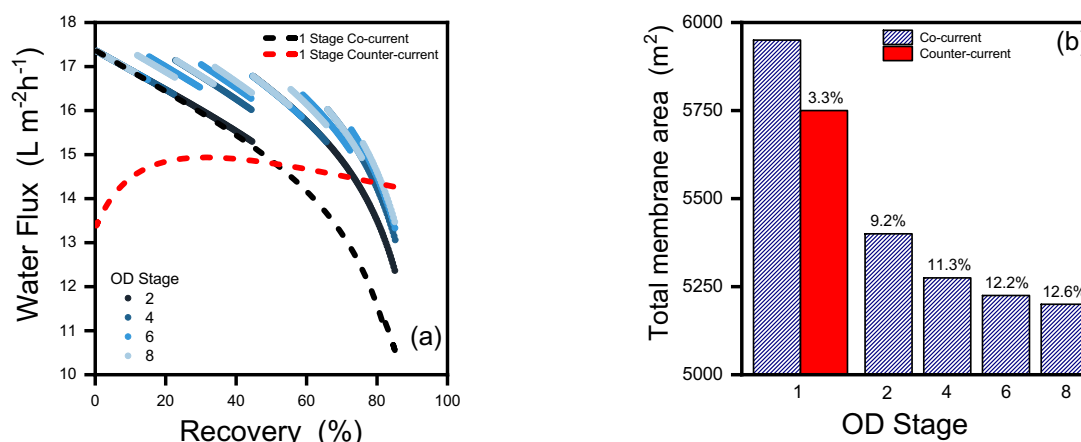


Fig. 3. Model results for the ODCW, considering the system based on the second configuration investigated (Conf2). The simulations were performed considering an influent seawater DS volume of  $200 \text{ m}^3 \text{ h}^{-1}$  entering each stage with a target recovery rate of 85 % for the overall system. Results are presented for both co-current and counter-current permeation modes. Panel a) presents the water flux trend as function of the recovery rate while varying the number of stages in co-current system design. Dashed lines represent the co-current and counter-current simulations performed with single stage design. Panel b) presents the variation of the membrane area required to achieve the target recovery rate, as function of the number of stages in the osmotic dilution system.

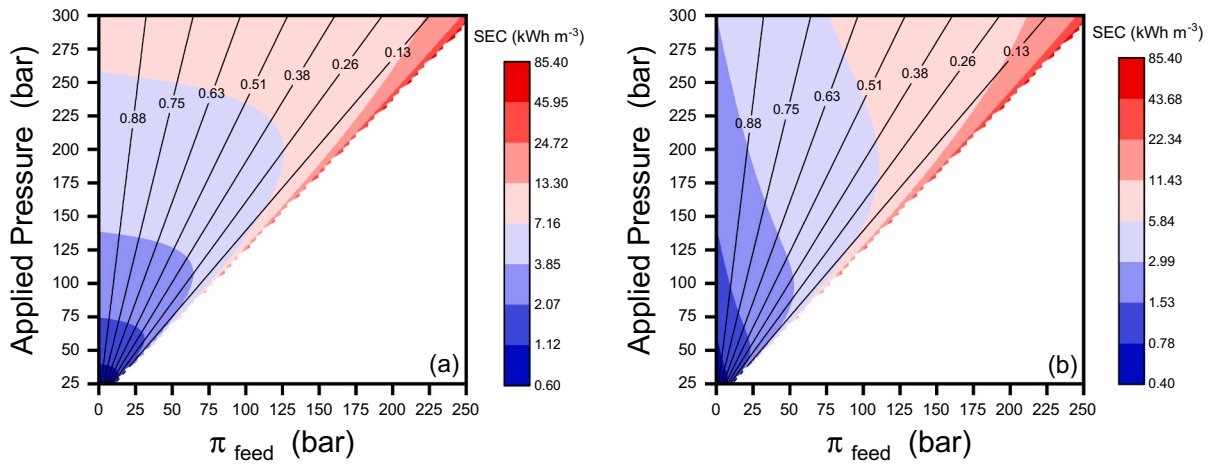
### 3.4. RO simulations – SEC

Fig. 4 shows the specific thermal energy consumption  $SEC_I$  of RO used as downstream desalination technology for the draw solution regeneration.  $SEC_I$  is reported as function of the inlet osmotic pressure of the feed solution to be treated (i.e.,  $\pi_{feed}$ ) and of the water recovery. The latter is denoted by continuous black lines. In detail,  $SEC_I$  values related to the single-stage uniform pressure configuration and to the multi-stage configuration are reported on the left (Fig. 4a) and on the right (Fig. 4b) of the panel, respectively. Without losing generality, the results in Fig. 4b refer to the configuration with 3 stages in series.

The hydraulic pressure applied, evaluated by exploiting Eqs. 4 and 7, is reported on the y-axis. These pressure values correspond, applying the appropriate unit conversions, to  $SEC_I$ . As the applied hydraulic pressure increases, the range of solutions that can be treated widens (namely,  $\pi_{feed}$  increases), although with different water recoveries  $R$ , which are inversely proportional to the inlet osmotic pressure (i.e.,  $\pi_{feed}$ ).

Calculations were performed considering applied hydraulic pressures between 25 and 300 bar, thus also covering unconventional high-pressure reverse osmosis systems. Moreover,  $\Delta p_{out}$ ,  $\eta_{pump}$ ,  $\eta_{ERD}$  and the salt rejection were assumed equal to 10 bar, 0.8, 0.9 and 100 %, respectively. The  $SEC_I$  calculated for single-stage RO (e.g., when the maximum applied pressure is equal to 80 bar [23]) ranges from 2.22 to  $10.4 \text{ kWh m}^{-3}$ . In this scenario, the water recovery  $R$  ranges from 0.98 to 0.03 and  $\pi_{feed}$  from 1 to  $\approx 60.4$  bar, which corresponds to a concentration of 72 and  $78 \text{ g L}^{-1}$  in case of NaCl and  $\text{MgCl}_2$  aqueous solutions, respectively. When the applied pressure is instead equal to 25 bar, the  $SEC_I$  ranges from 0.70 to  $0.91 \text{ kWh m}^{-3}$ , which corresponds to a water recovery equal to 0.92 and 0.24 and a  $\pi_{feed}$  equal to 1 and 9.48 bar, respectively. In case of HPRO, i.e., when the applied pressure ranges from 150 to 300 bar, the  $SEC_I$  may reach improbable values of about  $85.4 \text{ kWh m}^{-3}$ . At the lower boundary of this operating range, the maximum osmotic pressure of the feed solution is about 124 bar ( $0.02 \leq R \leq 0.99$ ), whilst at the upper boundary  $\pi_{feed}$  may reach values slightly higher than 250 bar ( $0.02 \leq R \leq 0.99$ ). Note that a cut-off value for recovery ratio of 0.01 was set, due to the lack of engineering interest of conditions beyond this threshold.

In Fig. 4b, the  $SEC_I$  of the multi-stage configuration is reported. As expected, compared to the single-stage RO, the calculated  $SEC_I$  is lower, under the same  $R$  and  $\pi_{feed}$  values. In fact, the reverse osmosis process is divided into several stages characterized by a different and gradually increasing hydraulic pressure, according to the increasing concentration



**Fig. 4.** Specific thermal energy consumption ( $SEC_I$ ) as function of the inlet osmotic pressure of the feed solution to be treated (i.e.,  $\pi_{feed}$ ) and the water recovery (see black lines), in case of a) single-stage uniform pressure and b) 3-stage RO process configuration. The maximum applied hydraulic pressure reported on the y-axis corresponds to the  $SEC_I$ . Calculations were performed considering the maximum applied hydraulic pressure ranges between 25 and 300 bar (thus also covering high-pressure reverse osmosis systems) and, thus,  $\pi_{feed}$  between 1 and 250 bar. Then,  $\Delta p_{out}$ ,  $\eta_{pump}$ ,  $\eta_{ERD}$  and the salt rejection were assumed equal to 10 bar, 0.8, 0.9 and 100 %, respectively.

of the treated solution. In case of 3-stage RO, the calculated  $SEC_I$  ranges from 0.99 to 10.4  $\text{kWh m}^{-3}$ , considering a value of 80 bar. In this scenario, the water recovery  $R$  ranges from 0.98 to 0.03 and  $\pi_{feed}$  from 1 to  $\approx 60.4$  bar, as in case of a single stage. When the applied pressure is equal to 25 bar, the  $SEC_I$  ranges from 0.48 (i.e. a 30 % reduction compared to the single-stage configuration) to 0.88  $\text{kWh m}^{-3}$  (i.e. a 4 % reduction compared to the single-stage configuration), which corresponds to a water recovery equal to 0.92 and 0.24 and a  $\pi_{feed}$  equal to 1 and 9.48 bar, respectively.

In case of HPRO, the maximum  $SEC_I$  occurs for significantly lower recoveries. In this scenario, the difference between the 3-stage and single stage case is minimal and below 1 %. As we move towards higher recoveries, the reduction in the energy consumption may reach up to 60 %. In particular, when the applied pressure is equal to 150 bar, the  $SEC_I$  varies from 1.66 to 26.0  $\text{kWh m}^{-3}$ , thus yielding energy savings of 60 % and 1 % in the case of lower and higher concentrated aqueous solutions, respectively. Finally, it is worth emphasising that the electrical energy exploited to power the RO is in theory totally convertible to work, thus the specific exergy consumption  $SEC_{II}$  corresponds exactly to  $SEC_I$ .

### 3.5. MD simulations – SEC

In Fig. 5a, the specific energy consumption ( $SEC_I$ ) of an MD process used as downstream desalination technology for the draw solution regeneration is reported as function of the temperature difference between inlet feed and permeate channel flows ( $\Delta T$ ) and the thermal efficiency ( $\eta_{mem}$ ). Same results are reported in details in Fig. S6 a and c of the Supporting Information. In the analysis,  $\Delta T$  ranges between 10°C and 65°C, while  $\eta_{mem}$  between 0.4 and 1 [32]. In case of simple configuration without the HX, the  $SEC_I$  ranges from 2210 to 1860  $\text{kWh m}^{-3}$  when  $\Delta T$  is equal to 10 and 65°C, respectively, and considering  $\eta_{mem}$  equal to 0.4. Assuming an ideal  $\eta_{mem} = 1$ , the  $SEC_I$  decreases to the following values: 884 to 744  $\text{kWh m}^{-3}$  in case of  $\Delta T$  equal to 10 and 65°C, respectively. On the other hand, if a HX is included, the three-dimensional curve describing the potential  $SEC_I$  moves downwards and exhibits a more pronounced influence of  $\Delta T$ , since the latter determines the amount of heat that can be recovered before achieving thermal equilibrium with the environment. In detail,  $SEC_I$  ranges from 894 to 183  $\text{kWh m}^{-3}$  for  $\eta_{mem}$  equal to 0.4 and  $\Delta T$  equal to 10 and 65°C, respectively. For  $\eta_{mem}$

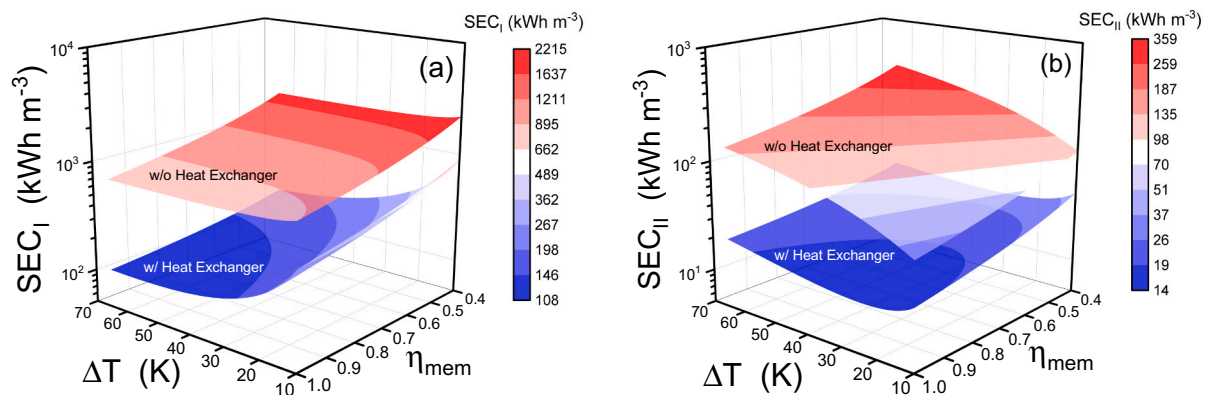


**Fig. 5.** Specific thermal a) energy ( $SEC_I$ ) and b) exergy ( $SEC_{II}$ ) consumption of MD as function of the temperature difference between inlet feed and permeate channel flows  $\Delta T$  and the thermal efficiency  $\eta_{mem}$ . Calculations were performed considering both the configuration introduced in Fig. 1, namely: a configuration without heat recovery (see Fig. 1a), and a more efficient configuration where heat recovery is accomplished by means of a heat exchanger (see Fig. 1b). In the analysis,  $\Delta T$  ranges between 10 and 65°C, while  $\eta_{mem}$  between 0.4 and 1 [32]. Then,  $\Delta T_{HX}$  and  $\Delta T_{MD, f, in}$  were assumed equal to 2°C;  $T_C$  equal to 20°C and the specific heat was considered temperature and concentration dependent (without losing generality,  $c_f$  is referred to an aqueous solution of  $\text{MgCl}_2$ ). Finally,  $\Delta T_S$ , exploited to evaluate  $\eta_{Carnot}$  and thus the  $SEC_{II}$ , was assumed equal to 5°C.

equal to 1, it ranges from 363 to 110 kWh m<sup>-3</sup>. As a result, depending on the choice of the operating parameters (namely,  $\eta_{mem}$  and  $\Delta T$ ), the energy savings in case of heat recovery range from 60 to 90 % with respect to the case without the HX.

Similarly, the related exergy performance  $SEC_{II}$  is reported in Fig. 5b), being  $SEC_{II} = SEC_I \eta_{Carnot}$ . The Carnot efficiency is evaluated

using Eq. 16 and ranges from 0.05 to 0.19 in case of  $\Delta T$  equal to 10 and 65°C, respectively. Same results are reported in details in Fig. S6 b and d of the Supporting Information.

Differently from RO, the exergy consumption of MD to produce a unit volume of distillate is lower than the energy consumption, thanks to the possibility of harnessing low-temperature waste heat sources. The

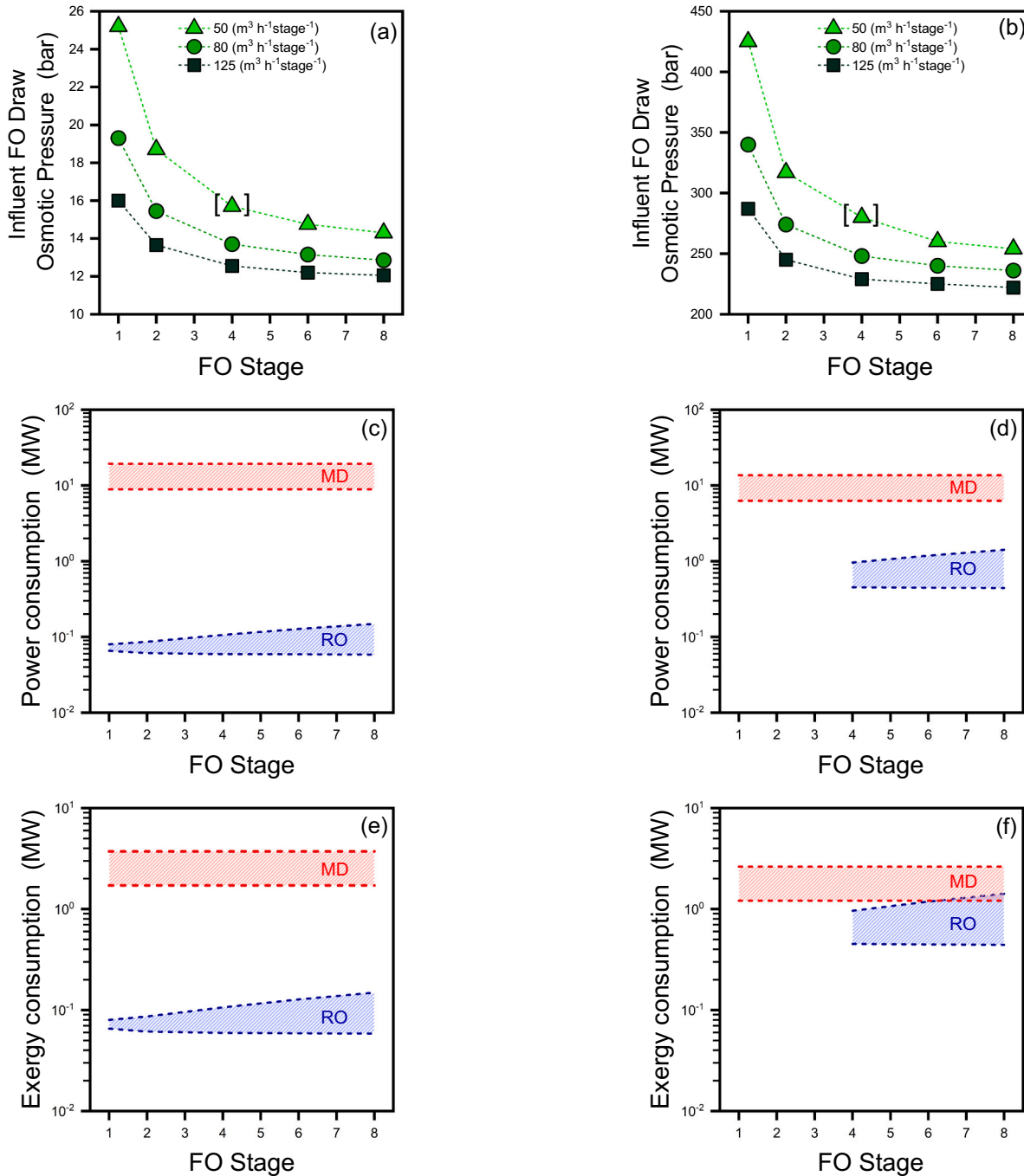


**Fig. 6.** Investigation of the coupling between FO and downstream desalination systems, represented by either RO or MD. The influent DS osmotic pressure is reported as a function of the number of FO stages considering a) FOCW and b) FOHW scenarios. FO simulations were performed by changing the influent DS flow rate per stage. Each square, circle and triangle in a) and b) represent a specific FO system. Triangles reported in squared brackets are representative of the case study presented in Figs. 2 and 3, where a draw solution to feed solution flow rate ratio equal to 2 to 1 was deployed. Panels c) and d) are referred to the power consumption of reverse osmosis and membrane distillation coupled with forward osmosis, whilst panels e) and f) to the related exergy consumption. Results are reported as a function of the number of stages implemented in FO, considering an influent volume flow rate of 80 m<sup>3</sup> h<sup>-1</sup> stage<sup>-1</sup>. Left panels refer to the FO-RO/MD applied for civil wastewater treatment, while right panels refer to FO-RO/MD applied for treating hypersaline solutions. Note that, in the hypersaline case  $c_p/c_f$  was artificially set equal to 1, for simplicity. The reason for this choice is merely related to the unavailability of correlations describing the dependence of specific heat on concentration of NaPRO at high concentrations.

configuration without HX shows exergy consumption yields ranging from 108 to 358 kWh m<sup>-3</sup> in case of  $\eta_{mem} = 0.4$ , and from 43.0 to 143 kWh m<sup>-3</sup> in case of  $\eta_{mem} = 1$  ( $10^{\circ}\text{C} \leq \Delta T \leq 65^{\circ}\text{C}$ ). The configuration with the HX shows exergy consumption ranging from 43.5 to 35.2 kWh m<sup>-3</sup> in case of  $\eta_{mem} = 0.4$ , and from 17.7 to 21.3 kWh m<sup>-3</sup> in case of  $\eta_{mem} = 1$  ( $10^{\circ}\text{C} \leq \Delta T \leq 65^{\circ}\text{C}$ ).

### 3.6. Envisioned coupling - energy demand

Additional calculations were performed to investigate the coupling of FO with the considered desalination systems for draw solution regeneration. The results are reported in Fig. 6. The analysis focused on evaluating the power and the related exergy needs to drive the potential downstream desalination system, consisting of either a pressure- or a thermally-driven membrane process, i.e., reverse osmosis or membrane distillation. Since the energy required by the post-process is strongly associated with the influent (i) DS osmotic pressure and (ii) DS flow rate required to drive the permeation in the forward osmosis step, a first set of simulations investigated the variation of these parameters in single or multiple stage FO operation. It is worth noting that the simulations were performed in accordance with the modeling analysis described above, considering the treatment of a fixed amount of feed solution equal to 100 m<sup>3</sup> h<sup>-1</sup>. The simulations were performed considering Conf2 as multi-stage FO operation, accounting for the promising results reported in the previous sections.

The results are reported in Fig. 6a and b for the FOCW and FOHW scenario, respectively. Each square, circle or triangle refers to a specific FO system, designed for either wastewater (Fig. 6a) or hypersaline (Fig. 6b) water treatment. The modeling analysis was performed by increasing the total DS flow rate according to the number of stages involved, considering three alternatives: 50, 80, and 125 m<sup>3</sup> h<sup>-1</sup> per stage. For example, the triangle related to three FO stages means that 150 m<sup>3</sup> h<sup>-1</sup> of draw solution is used in the system per each 50 m<sup>3</sup> h<sup>-1</sup> entering one of the stage, and so on. Different flow rate ranges were studied with the aim to understand the relative variation of the influent DS osmotic pressures.

As expected, by increasing the number of FO stages (and hence the total DS flow rate deployed in the system), lower influent DS osmotic pressures are needed to reach the same water recovery. However, the results suggest the existence of a trade-off, where a multiple permeation system with more than 8 FO stages would not necessarily translate into significant reductions in the influent DS osmotic pressure (hence, draw solute concentration).

On the other hand, a near-exponential trend may be observed while decreasing the number of stages below roughly 4. As expected, larger concentrations of draw solute are necessary to compensate the larger dilution factor of lower DS flow rates during the FO permeation. For instance, increasing the number of stages from 1 to 4, thus multiplying the total DS flow rates by 4, would require reducing the influent osmotic pressure by 30–40 %, from 26 to 16 bar when treating wastewater, and from 430 to 290 bar when treating hypersaline water sources. That also means that the total mass flow rate of DS would be higher at increased number of stages. It is worth mentioning that the simulations were performed in co-current and similar discussions are no more valid for counter-current systems, where a multiple stage approach would not report a potential benefits in filtration conditions.

The analysis of the power associated with the deployment of different downstream desalination systems (RO vs. MD) while varying the operating parameters in forward osmosis is reported in Fig. 6c, d), e) and f). The results were computed considering an influent DS volume per stage equal to 80 m<sup>3</sup> h<sup>-1</sup> and the relative FO recovery rates considering the FOCW and FOHW scenarios, i.e., 85 % and 60 %, respectively. The subsequent RO or MD systems were designed to process the diluted draw solution coming from the FO unit, with the goal of extracting the relative high-quality water filtered during the FO step. The energy and exergy analyses performed to investigate the coupling of

RO or MD with FO in the case of the deployment of 50 or 125 m<sup>3</sup> h<sup>-1</sup> stage<sup>-1</sup> are reported in the Supporting Information (Figs. S7 and S8).

In detail, Fig. 6c) and d) refer to the power consumption, while Fig. 6e) and f) to the exergy consumption in case of wastewater and hypersaline water treatment, respectively. The blue areas illustrate the power or exergy demand in the case of 3-stage RO process as a function of the number of implemented FO stages. The dashed lines delimiting such areas refer to  $\eta_{ERD} = 1$  (lower dashed line) and  $\eta_{ERD} = 0.8$  (upper dashed line). Similarly, the red areas refer to power and exergy demands when using the MD process to regenerate the draw solution. The dashed lines delimiting the red areas are drawn considering the standard deviation, which results from efficiency variation in the range  $0.4 \leq \eta_{mem} \leq 1$ . In these calculations,  $\Delta T$  is kept equal to 65°C.

In case of wastewater (see Fig. 6c), the 3-stage RO power consumption ranges from 65.4 kW ( $\eta_{ERD} = 1$ ) to 79.9 kW ( $\eta_{ERD} = 0.8$ ) when the FO process involves a single stage, and from 58.5 kW ( $\eta_{ERD} = 1$ ) to 149 kW ( $\eta_{ERD} = 0.8$ ) when the FO process involves 8 stages. This difference is ultimately due to the larger draw solute mass involved in a multi-stage FO operation, i.e., higher flow rate and/or osmotic pressure that needs to be processed in RO, as indicated above. On the other hand, the MD process requires  $14.1 \pm 5.21$  MW (the power consumption is indicated as average value  $\pm 1$  s.d.), in accordance to the fact that MD is a more energy-intensive process. Hypersaline solutions (see Fig. 6d) can be regenerated by a RO processes, but solely when the number of FO stages is more than 4, i.e., in cases whereby the osmotic pressure of the draw solution is relatively low (i.e. restricted to the FOHW case under consideration). When the FO stages are lower than 4, this coupling turns out to be not feasible. As a matter of fact, if the number of FO stages is reduced, the volume of draw solution entering the RO module also decreases while increasing the target recovery in percentage (all other chemical and physical operating conditions being equal). It is worth noting that a maximum applied pressure of 300 bar was considered here, well above the pressures exploited in operational plants. This represents a challenge considering the membrane material and the design of the module [23]. The RO power demand ranges from 0.45 ( $\eta_{ERD} = 1$ ) to 0.96 ( $\eta_{ERD} = 0.8$ ) MW, and from 0.44 ( $\eta_{ERD} = 1$ ) to 1.41 ( $\eta_{ERD} = 0.8$ ) MW, in case of 4 and 8 FO stages, respectively. On the other hand, MD, although less efficient, turns out to be a more flexible process with a wider range of application. The reason lies in its being a process which occurs at ambient pressure. The MD process requires  $9.95 \pm 3.68$  MW.

As discussed previously, exergy (see Fig. 6e and f) and power consumption remain unaltered in the RO case, while MD exergy consumption is reduced by about 80 % in both wastewater and hypersaline cases because of the Carnot factor. In detail, the MD exergy consumption is  $2.72 \pm 1.00$  MW and  $1.92 \pm 0.71$ , in case of wastewater (see Fig. 6e) and hypersaline solutions (see Fig. 6f), respectively.

Finally, it is worth noting that the maximum recovery achievable in a single MD stage is, at best, 10 % (see Fig. S5). Therefore, leveraging the action of multiple MD stages placed in series is essential to achieve recoveries higher than 10 %. In this work, we have assumed that each of the MD stages in series requires the same energy consumption, whose value lies in the red areas (see Fig. 6).

## 4. Discussions and conclusions

This study reports a comprehensive modeling analysis of forward osmosis and its coupling with pressure- and thermally-driven downstream desalination technologies. The study was performed focusing on the energy needs associated with the production of clean water according to different operating modes.

First, a system-scale modeling of FO was carried out also evaluating two configurations for large-scale applications, characterized by a multi-stage operation approach. This was done to understand potential savings or optimization in terms of distribution of driving force within the system. In the model, the flow rates and osmotic pressures of the draw solution were varied. Each of these operating condition leads to different

energy requirements for the downstream RO or MD steps. Substantial differences were observed depending on the feed solution composition and the chosen application, i.e., forward osmosis or osmotic dilution.

In the case of FO deployed for treating of civil wastewater sources, results suggest that working with membrane modules in co-current may result in a versatile filtration system, thanks to the possibility to operate in multiple stages, which instead is not advantageous in counter-current. The single-stage counter current mode represents the best solution in a traditional configuration (single-stage approach) thanks to the more uniform concentration gradients achieved between the feed and the draw solution within the system. However, this performance may be obtained only by properly setting the operative limits of the relative membrane modules. On the other hand, a significant variability in water permeation rate may be observed both in co-current (single and multi-stage) and counter-current (single stage) modes in the treatment of hypersaline solutions. This may be ascribed to the large variation in concentration of feed and draw solutions along the membrane modules, translating into potential issues for real-scale operation. By maintaining unaltered the water extraction capacity in FO, a multi-stage operation may be characterized by significant savings in terms of draw solute concentration, i.e. osmotic pressure, potentially followed by easier system maintenance, thus lowering the environmental and operative costs of the filtration process. In co-current mode, a multi-stage process would be also beneficial by working in osmotic dilution mode with natural DS (seawater) for the extraction of clean water from civil wastewater, resulting in an increase in water recovery while reducing the footprint of the filtration system. However, this can be obtained only at the expense of the deployment of a larger DS flow rate.

Then, reverse osmosis and membrane distillation were investigated as potential downstream desalination systems for the regeneration of the draw solution, while simultaneously extracting the clean water previously filtered in the FO step. First, energy and exergy analyses were performed to study the influence of the operating parameters in pressure- and thermally- driven membrane systems, separately. Overall, results suggest that the configuration of the subsequent desalination system may strongly affect its energy consumption. In reverse osmosis, a multi-stage operation would result in a significant *SEC* reduction compared to the 1-stage RO system, mostly when working at higher recovery rates or larger applied pressures. The analysis was performed considering also unconventional operating parameters, i.e., applied pressure above 150 bar, thus covering future potential membrane and module development. Looking at this high-pressure RO configuration, the maximum *SEC* occurs for significantly low water recoveries. In this scenario, the difference between the 3 stage and single stage case is minimal and below 1 %. At higher recovery rates, the reduction in the specific energy consumption may reach up to 60 %.

Then, two different MD configurations were investigated, considering the possible implementation of a heat exchanger (HX) to partially recover the heat losses. Without the HX, the energy consumption is dictated by the intrinsic efficiency of the membrane, while in MD systems incorporating HXs, the *SEC* is strongly influenced by the resulting temperature difference at the membrane surface, since this determines the amount of heat that can be recovered before achieving thermal equilibrium with the environment. Therefore, it is of paramount importance to highlight that new and innovative membrane materials for MD applications should be developed hand in hand with an in-depth understanding of the module and system configuration.

When studying the coupling of FO with RO or MD, the analysis showed that an FO-MD configuration would result in a less energy-efficient technology than the FO-RO case. This was somehow expected, considering the intrinsic nature of the two downstream desalination systems, i.e., MD vs. RO. Interestingly, the FO-MD system is a more flexible process, with a wider range of application. This is mostly ascribed to the possibility of working with extended salinity levels. Indeed, the treatment of hypersaline solutions in FO at fixed recovery rates can be accomplished by working with low DS volumes only by

drastically increasing the influent DS osmotic pressure, and the resulting diluted draw solution can be handled only via the thermally-driven membrane system. For this specific application, reverse osmosis can be deployed only in combination with a multi-stage FO, where a decrease in the required DS osmotic pressure is counter-posed by an increase of its total influent flow rate. However, the exergetic analysis showed that no substantial difference would be observed between the implementation of an FO-MD or FO-RO process, differently from what observed in the treatment of wastewater sources. For the latter, the combination of forward osmosis with pressure-driven membrane processes results as the best technological option, with an overall specific energy consumption two orders of magnitude lower than that needed to drive an FO-MD system.

#### CRediT authorship contribution statement

**Mattia Giagnorio:** Conceptualization, Methodology, Software, Validation, Formal analysis, Investigation, Resources, Data curation, Writing – original draft, Writing – review & editing, Visualization, Supervision, Project administration. **Matteo Morciano:** Conceptualization, Methodology, Software, Validation, Formal analysis, Investigation, Resources, Data curation, Writing – original draft, Writing – review & editing, Visualization, Supervision, Project administration. **Wenjing Zhang:** Writing – review & editing. **Claus Hélix-Nielsen:** Writing – review & editing. **Matteo Fasano:** Investigation, Writing – original draft, Writing – review & editing, Data curation. **Alberto Tiraferri:** Investigation, Writing – original draft, Writing – review & editing, Data curation.

#### Declaration of competing interest

The authors declare that they have no known competing financial interests or personal relationships that could have appeared to influence the work reported in this paper.

#### Data availability

Data will be made available on request.

#### Acknowledgments

M.G., W.Z. and C.H.N. thank the Department of Environmental and Resource Engineering. M.M., M.F. and A.T. thank the CleanWaterCenter@PoliTo.

#### Appendix A. Supplementary data

Supplementary data to this article can be found online at <https://doi.org/10.1016/j.desal.2022.116083>.

#### References

- [1] T.Y. Cath, A.E. Childress, M. Elimelech, Forward osmosis: principles, applications, and recent developments, *J. Membr. Sci.* 281 (1–2) (2006) 70–87.
- [2] K. Lutchmiah, A. Verliedje, K. Roest, L.C. Rietveld, E. Cornelissen, Forward osmosis for application in wastewater treatment: a review, *Water Res.* 58 (2014) 179–197.
- [3] B.D. Coday, N. Almaraz, T.Y. Cath, Forward osmosis desalination of oil and gas wastewater: impacts of membrane selection and operating conditions on process performance, *J. Membr. Sci.* 488 (2015) 40–55.
- [4] M. Li, K. Li, L. Wang, X. Zhang, Feasibility of concentrating textile wastewater using a hybrid forward osmosis-membrane distillation (FO-MD) process: performance and economic evaluation, *Water Res.* 172 (2020), 115488.
- [5] A. Mahto, K. Aruchamy, R. Meena, M. Kamali, S.K. Nataraj, T.M. Aminabhavi, Forward osmosis for industrial effluents treatment–sustainability considerations, *Sep. Purif. Technol.* 254 (2021), 117568.
- [6] Y. Li, Z. Xu, M. Xie, B. Zhang, G. Li, W. Luo, Resource recovery from digested manure centrate: comparison between conventional and aquaporin thin-film composite forward osmosis membranes, *J. Membr. Sci.* 593 (2020), 117436.

- [7] J. Zhang, D. Wang, Y. Chen, B. Gao, Z. Wang, Scaling control of forward osmosis-membrane distillation (FO-MD) integrated process for pre-treated landfill leachate treatment, *Desalination* 520 (2021), 115342.
- [8] M.S. Nawaz, H.S. Son, Y. Jin, Y. Kim, S. Soukane, M.A. Al-Hajji, M. Abu-Ghdaib, N. Ghaffour, Investigation of flux stability and fouling mechanism during simultaneous treatment of different produced water streams using forward osmosis and membrane distillation, *Water Res.* 198 (2021), 117157.
- [9] S.J. Im, L. Fortunato, A. Jang, Real-time fouling monitoring and membrane autopsy analysis in forward osmosis for wastewater reuse, *Water Res.* 197 (2021), 117098.
- [10] A.J. Ansari, F.I. Hai, W.E. Price, J.E. Drewes, L.D. Nghiem, Forward osmosis as a platform for resource recovery from municipal wastewater—a critical assessment of the literature, *J. Membr. Sci.* 529 (2017) 195–206.
- [11] S. Phuntsho, H.K. Shon, S. Hong, S. Lee, S. Vigneswaran, A novel low energy fertilizer driven forward osmosis desalination for direct fertigation: evaluating the performance of fertilizer draw solutions, *J. Membr. Sci.* 375 (1–2) (2011) 172–181.
- [12] D. Li, H. Wang, Smart draw agents for emerging forward osmosis application, *J. Mater. Chem. A* 1 (45) (2013) 14049–14060.
- [13] M. Zhan, Y. Kim, S. Hong, Comprehensive review of osmotic dilution/concentration using FO membranes for practical applications, *Desalination* 515 (2021), 115190.
- [14] L. Francis, F.E. Ahmed, N. Hilal, Advances in membrane distillation module configurations, *Membranes* 12 (1) (2022) 81.
- [15] S.M. Ali, S.-J. Im, A. Jang, S. Phuntsho, H.K. Shon, Forward osmosis system design and optimization using a commercial cellulose triacetate hollow fibre membrane module for energy efficient desalination, *Desalination* 510 (2021), 115075.
- [16] M. Giagnorio, F. Ricceri, A. Tiraferri, Desalination of brackish groundwater and reuse of wastewater by forward osmosis coupled with nanofiltration for draw solution recovery, *Water Res.* 153 (2019) 134–143.
- [17] G.Q. Chen, A. Artemi, J. Lee, S.L. Gras, S.E. Kentish, A pilot scale study on the concentration of milk and whey by forward osmosis, *Sep. Purif. Technol.* 215 (2019) 652–659.
- [18] M.N. Fini, H.T. Madsen, J.L. Sørensen, J. Muff, Moving from lab to pilot scale in forward osmosis for pesticides rejection using aquaporin membranes, *Sep. Purif. Technol.* 240 (2020), 116616.
- [19] W.V. Anderson, C.-M. Cheng, T.S. Butalia, L.K. Weavers, Forward osmosis–membrane distillation process for zero liquid discharge of flue gas desulfurization wastewater, *Energy Fuel* 35 (6) (2021) 5130–5140.
- [20] D.L. Shaffer, J.R. Werber, H. Jaramillo, S. Lin, M. Elimelech, Forward osmosis: where are we now? *Desalination* 356 (2015) 271–284.
- [21] A. Deshmukh, C. Boo, V. Karanikola, S. Lin, A.P. Straub, T. Tong, D.M. Warsinger, M. Elimelech, Membrane distillation at the water-energy nexus: limits, opportunities, and challenges, *Energy Environ. Sci.* 11 (5) (2018) 1177–1196.
- [22] T. Tong, M. Elimelech, The global rise of zero liquid discharge for wastewater management: drivers, technologies, and future directions, *Environ.Sci.Technol.* 50 (13) (2016) 6846–6855.
- [23] D.M. Davenport, A. Deshmukh, J.R. Werber, M. Elimelech, High-pressure reverse osmosis for energy-efficient hypersaline brine desalination: current status, design considerations, and research needs, *Environ.Sci.Technol.Lett.* 5 (8) (2018) 467–475.
- [24] X. Wu, C.H. Lau, B.K. Pramanik, J. Zhang, Z. Xie, State-of-the-art and opportunities for forward osmosis in sewage concentration and wastewater treatment, *Membranes* 11 (5) (2021) 305.
- [25] E. Chiavazzo, M. Morciano, F. Viglino, M. Fasano, P. Asinari, Passive solar high-yield seawater desalination by modular and low-cost distillation, *Nat.Sustain.* 1 (12) (2018) 763–772.
- [26] M. Morciano, M. Fasano, S.V. Boriskina, E. Chiavazzo, P. Asinari, Solar passive distiller with high productivity and marangoni effect-driven salt rejection, *Energy Environ. Sci.* 13 (10) (2020) 3646–3655.
- [27] A. Najib, J. Orfi, E. Ali, J. Saleh, Thermodynamics analysis of a direct contact membrane distillation with/without heat recovery based on experimental data, *Desalination* 466 (2019) 52–67.
- [28] A. Najib, J. Orfi, H. Alansary, E. Ali, Assessing the impact of operating conditions on the energy and exergy efficiency for multi-effect vacuum membrane distillation systems, *Water* 13 (11) (2021) 1500.
- [29] G. Antonetto, M. Morciano, M. Alberghini, G. Galgaroli, A. Ciocia, L. Bergamasco, F. Spertino, M. Fasano, Synergistic freshwater and electricity production using passive membrane distillation and waste heat recovered from camouflaged photovoltaic modules, *J. Clean. Prod.* 318 (2021), 128464.
- [30] S. Al-Obaidani, E. Curcio, F. Macedonio, G. Di Profio, H. Al-Hinai, E. Drioli, Potential of membrane distillation in seawater desalination: thermal efficiency, sensitivity study and cost estimation, *J. Membr. Sci.* 323 (1) (2008) 85–98.
- [31] M. Xie, L.D. Nghiem, W.E. Price, M. Elimelech, A forward osmosis–membrane distillation hybrid process for direct sewer mining: system performance and limitations, *Environ.Sci.Technol.* 47 (23) (2013) 13486–13493.
- [32] A. Deshmukh, M. Elimelech, Understanding the impact of membrane properties and transport phenomena on the energetic performance of membrane distillation desalination, *J. Membr. Sci.* 539 (2017) 458–474.
- [33] K.S. Bowden, A. Achilli, A.E. Childress, Organic ionic salt draw solutions for osmotic membrane bioreactors, *Bioresour. Technol.* 122 (2012) 207–216.
- [34] A. Achilli, T.Y. Cath, A.E. Childress, Selection of inorganic-based draw solutions for forward osmosis applications, *J. Membr. Sci.* 364 (1–2) (2010) 233–241.
- [35] R.W. Holloway, R. Maltos, J. Vanneste, T.Y. Cath, Mixed draw solutions for improved forward osmosis performance, *J. Membr. Sci.* 491 (2015) 121–131.
- [36] M.S. Islam, S. Sultana, J.R. McCutcheon, M.S. Rahaman, Treatment of fracking wastewaters via forward osmosis: evaluation of suitable organic draw solutions, *Desalination* 452 (2019) 149–158.
- [37] K.L. Hickenbottom, T.Y. Cath, Sustainable operation of membrane distillation for enhancement of mineral recovery from hypersaline solutions, *J. Membr. Sci.* 454 (2014) 426–435.
- [38] K.S. Christie, T. Horsemann, S. Lin, Energy efficiency of membrane distillation: simplified analysis, heat recovery, and the use of waste-heat, *Environ. Int.* 138 (2020), 105588.
- [39] M. Giagnorio, F. Ricceri, M. Tagliabue, L. Zaninetta, A. Tiraferri, Hybrid forward osmosis–nanofiltration for wastewater reuse: system design, *Membranes* 9 (5) (2019) 61.
- [40] M. Giagnorio, A. Casasso, A. Tiraferri, Environmental sustainability of forward osmosis: the role of draw solute and its management, *Environ. Int.* 152 (2021), 106498.
- [41] V. Yangali-Quintanilla, Z. Li, R. Valladares, Q. Li, G. Amy, Indirect desalination of red sea water with forward osmosis and low pressure reverse osmosis for water reuse, *Desalination* 280 (1–3) (2011) 160–166.
- [42] Z.M. Binger, A. Achilli, Forward osmosis and pressure retarded osmosis process modeling for integration with seawater reverse osmosis desalination, *Desalination* 491 (2020), 114583.
- [43] A. Tiraferri, N.Y. Yip, A.P. Straub, S.R.-V. Castrillon, M. Elimelech, A method for the simultaneous determination of transport and structural parameters of forward osmosis membranes, *J. Membr. Sci.* 444 (2013) 523–538.
- [44] S. Lin, M. Elimelech, Staged reverse osmosis operation: configurations, energy efficiency, and application potential, *Desalination* 366 (2015) 9–14.
- [45] Z. Cao, J. Deng, F. Ye, Cross-scale analysis of the energy recovery process in pressure exchanger and pipeline system, *Desalin. Water Treat.* 181 (2020) 151–160.
- [46] D.M. Warsinger, E.W. Tow, K.G. Nayar, L.A. Maswadeh, et al., Energy efficiency of batch and semi-batch (CCRO) reverse osmosis desalination, *Water Res.* 106 (2016) 272–282.
- [47] L. Wang, C. Violet, R.M. DuChanois, M. Elimelech, Derivation of the theoretical minimum energy of separation of desalination processes, *J. Chem. Educ.* 97 (12) (2020) 4361–4369.
- [48] A.J. Schunke, G.A. Hernandez Herrera, L. Padhye, T.-A. Berry, Energy recovery in SWRO desalination: current status and new possibilities, [Front. Sustain.](#) [Contribution](#) [Title](#) [Issue](#) [Series](#) [City](#) [Host](#) 2 (2020) 9.
- [49] A.P. Straub, A. Deshmukh, M. Elimelech, Pressure-retarded osmosis for power generation from salinity gradients: is it viable? *Energy Environ. Sci.* 9 (1) (2016) 31–48.
- [50] B. Peñate, L. García-Rodríguez, Energy optimisation of existing SWRO (seawater reverse osmosis) plants with ERT (energy recovery turbines): technical and thermoeconomic assessment, *Energy* 36 (1) (2011) 613–626.
- [51] M. Morciano, M. Fasano, L. Bergamasco, A. Albiero, M.L. Curzio, P. Asinari, E. Chiavazzo, Sustainable freshwater production using passive membrane distillation and waste heat recovery from portable generator sets, *Appl. Energy* 258 (2020), 114086.
- [52] F. Signorato, M. Morciano, L. Bergamasco, M. Fasano, P. Asinari, Exergy analysis of solar desalination systems based on passive multi-effect membrane distillation, *Energy Rep.* 6 (2020) 445–454.